In silico design of magnesium implants: macroscopic modelling

J.A. Sanz-Herrera [a] E. Reina-Romo [a] A.R. Boccaccini [b]

[a] *School of Engineering, University of Seville. Camino de los descubrimientos s/n, 41092 Seville, Spain. Tel.: +34 954 486079. Fax: +34 954 487295. E-mail: jsanz,erreina@us.es*

[b] *Institute of Biomaterials, Department of Materials Science and Engineering, University of Erlangen-Nuremberg*

Abstract

Magnesium-based biomedical implants offer many advantages versus traditional ones although some challenges are still present. In this context, mathematical modeling and computational simulation may be a useful and complementary tool to evaluate *in silico* the performance of magnesium biomaterials under different conditions. In this paper, a phenomenologically-based model to simulate magnesium corrosion is developed. The model describes the physico-chemical interactions and evolution of species present in this phenomenon. A set of 7 species is considered in the model, which allows to simulate hydrogen release, pH evolution, corrosion products formation as well as degradation of magnesium. The model is developed under the continuum media theory and is implemented in a finite element framework. In the results section, the effect of model parameters on outcomes is firstly explored. Second, model results are qualitative validated versus two examples of application found in the literature. Two main conclusions are derived from this work: (i) the model captures well the experimental trends and allows to analyze the main vari-

ables present in magnesium corrosion, (ii) even though further validation is needed the model may be a useful standard in the design of degradable metal implants.

Key words: Magnesium implants, Biodegradable metals, Tissue Engineering, Mathematical modeling, Computational simulation.

---

1 Introduction

1.1 Magnesium corrosion problem

Magnesium offers great advantages versus traditional implants, such as ceramics, polymers or metals, fundamentally due to: (i) it is biodegradable and hence a second removal surgery is not necessary, (ii) it shows similar mechanical properties than bone tissue avoiding stress shielding and osseointegration related problems, (iii) it can be used as a load bearing implant or tissue engineering scaffold application (4; 5; 18). Despite these features are known since the early use as a biomedical material in 1878 (34), there has been limited clinical application of magnesium as an implant solution since then to 2000s, probably due to limited knowledge of corrosion phenomenon and uncertain behavior under circumstances of uncontrolled degradation (29; 30). In the last 15 years there has been an exponential trend in the research of magnesium-based biomaterials which has provided better knowledge about the related physicochemical characterization of magnesium degradation and has shed light about the response of magnesium at different circumstances and applications (19). In parallel, many biomedical applications have been conceived and tested using magnesium biomaterials, such as cardiovascular stents (12; 25), bony implants (32; 37) or tissue engineering scaffolds (13; 30; 35), to cite a few.

Magnesium biomaterial behavior and time evolution is an extremely complex problem. Briefly, once the implant is immersed within an aqueous ionic solution, e.g. simulated body fluid (SBF) or *in vivo* environment, several ionic reactions are activated. Released ions interact with those present in the aqueous medium yielding to layer precipitation of corrosion products in the surface of the biomaterial and consumption of magnesium, i.e. degradation (33). It is clear that magnesium corrosion does not affect to implant mass loss by itself but also to the performance of mechanical properties such as stiffness, strength, toughness or fatigue resistance which are fundamental quantities for orthopedic applications (6; 15; 16; 17; 33).

Magnesium related problems are associated to uncontrolled degradation which derives in hydrogen release or pH amplification. On the one hand, hydrogen release gives place to the formation of a bubble which induces irregularities in implant-tissue interaction as well as the risk of explosion (21; 23). Indirectly, hydrogen release also induces a brittle mechanical behavior and decreases the fatigue resistance of the implant (6; 15; 16). On the other hand, pH alteration is an extremely dangerous issue in the human body although this risk is mitigated due to the buffer capacity *in vivo* (19).

In order to circumvent magnesium corrosion associated problems referred above, several strategies are adopted, namely, alloying and coating. Alloying and coating allow to tune degradation rate and corrosion performance of magnesium-based implants, and hence to get controlled release of hydrogen gas and hydroxil ions (19). Most popular magnesium alloys are based on Mg-Al, Mg-Zn, Mg-Ca and Mg-Rare earth elements (19). Some studies also reported on an enhanced osseointegration and osteoblast proliferation in the presence of certain alloys (7; 36). On contrary, magnesium alloys may present secondary

effects such as cytotoxicity or difficulty to evacuate alloy products from the human body (19; 33). On the other hand, surface modification and coating are usually performed by means of micro-arc oxidation, plasma spraying, hydrothermal method, electrochemical deposition, sol-gel deposition, chemical conversion coating deposition techniques (see (19) for a review). Localized break of the coated protective layer may induce an accelerated and localized corrosion in the biomaterial (pitting corrosion) (24).

1.2 Simulation of magnesium corrosion

There exists few models at the macroscale available to simulate degradation of magnesium biomaterials. Physically-based continuum models are presented in Grogan et al. (9; 10) with application to corrosion of metal stents. Recently, Bajger et al. (2) presented a similar model using a level-set strategy. However, these models consider a limited number of species and neglect the dynamics and evolution of secondary (although important) elements such as pH or corrosion products. A more detailed modeling of corrosion phenomena is necessary for the following reasons: (i) to properly describe the underlying physico-chemical features of corrosion phenomena and (ii) to get additional information and variables of analysis which may be compared by experimental outcomes.

1.3 Objectives and organization of the paper

The objective of the paper is the derivation of a complete and general mathematical model and its computational implementation, to simulate the degrada-

tion of magnesium biomaterials taking into consideration the physico-chemical interactions and evolution of the main involved species.

The paper is organized as follows: Firstly, the mathematical framework and model is introduced in the materials and methods section. Secondly, the results section shows an analysis of model parameters as well as qualitative validation of the model based on two examples found in the literature. Finally, a discussion of the results obtained from the model is established at the end of the paper.

2 Material and Methods

2.1 Species and evolution

Magnesium degradation is the result of the following chemical processes: (i) dissolution of magnesium in contact with an aqueous medium by means of ionic reactions, (ii) corrosion products formation in a surface layer and (iii) eventual layer dissolution in the presence of certain substances in the medium such as chloride. This process can be described by the following set of reaction equations (33):

$$Mg(s) + 2 \cdot H_2O(aq) \rightleftharpoons Mg^{2+}(aq) + H_2(g) + 2 \cdot OH^-(aq) \quad \text{Ionic reactions} \quad (1)$$

$$Mg^{2+}(aq) + 2 \cdot OH^{-}(aq) \rightleftharpoons MgO_2H_2(s) \quad \text{Corrosion products precipitation} \tag{2}$$

$$MgO_2H_2(s) + Cl^{-}(aq) \rightleftharpoons MgCl_2(s) + 2 \cdot OH^{-}(aq) \quad \text{Layer dissolution} \tag{3}$$

where aq, s and g refers to aqueous, solid and gas states of the species, see additionally Fig. 1. Eqs. (1) and (2) can be summarized in the following reaction:

$$Mg(s) + 2 \cdot H_2O(aq) \rightleftharpoons MgO_2H_2(s) + H_2(g) \quad \text{Magnesium degradation} \tag{4}$$

Reaction equations (3) and (4) are followed in the subsequent derivation of the theoretical framework. Therefore, 7 species are identified according to Fig. 1, namely:

- $[H_2O]$ [mol/m^3] aqueous species which represents water content present in the aqueous solution of the medium. It can diffuse into the porous materials of the corrosion products layer and magnesium biomaterial.
- $[Cl^{-}]$ [mol/m^3] aqueous species which represents chloride ions content present in the aqueous solution of the medium. It can diffuse into the porous materials of the corrosion products layer and magnesium biomaterial.
- $[H_2]$ [mol/m^3] gaseous species which represents hydrogen gas content produced as consequence of reaction (4). It can be encountered dissolved in the aqueous solution of the medium. It can diffuse into the porous materials of

the corrosion products layer and magnesium biomaterial.

- $[OH^-]$ [mol/m^3] aqueous species which represents hydroxide ions content produced as consequence of reaction (3). It can be encountered dissolved in the aqueous solution of the medium. It can diffuse into the porous materials of the corrosion products layer and magnesium biomaterial.
- $[Mg]$ [mol/m^3] solidus species which represents magnesium biomaterial.
- $[MgO_2H_2]$ [mol/m^3] solidus species which represents overall magnesium hydroxide produced as consequence of the balance between precipitation in reaction (4) and dissolution in reaction (3).
- $[MgCl_2]$ [mol/m^3] solidus species which represents magnesium chloride produced as consequence of precipitation in reaction (3).

The evolution of the kinetics of the involved species proceeds as follows. Both magnesium and magnesium hydroxide dissolution are considered to follow a first order kinetics as in other models (2; 27), such that:

$$[\dot{Mg}] = -k_d^{(1)} \cdot [Mg] \tag{5}$$

$$[\dot{MgO_2H_2}]_{diss} = -k_d^{(2)} \cdot [MgO_2H_2] \tag{6}$$

where $k_d^{(1)}$ and $k_d^{(2)}$ are the kinetic constants involved in eqs. (5) and (6), respectively (remark on the minus sign which denotes consumption). Then, having into consideration the stoichometry of reactions (3) and (4) yields,

$$[\dot{H_2O}] = 2 \cdot [\dot{Mg}] \tag{7}$$

$$[\dot{MgO_2H_2}]_{prec} = -[\dot{Mg}] \tag{8}$$

$$[\dot{H_2}] = -[\dot{Mg}] \tag{9}$$

$$[\dot{Cl^-}] = [\dot{MgO_2H_2}]_{diss} \tag{10}$$

$$[\dot{MgCl_2}] = [\dot{MgO_2H_2}]_{diss} \tag{11}$$

$$[\dot{OH^-}] = [\dot{MgO_2H_2}]_{diss} \tag{12}$$

Finally, $[MgO_2H_2] = [MgO_2H_2]_{diss} + [MgO_2H_2]_{prec}$.

2.2 Model

The model is established in the biomaterial domain $\Omega(\mathbf{x}, t)$, where $\mathbf{x}$ is the vector position of a material point of the domain and t represents time. This domain includes both magnesium implant bulk volume and surface layer. Aqueous species, represented by its density $\rho_{aq}(\mathbf{x}, t)$, can diffuse within the biomaterial. Therefore, in a control volume of the domain the net balance is stated as follows,

$$\dot{\rho}_{aq}(\mathbf{x}, t) = \dot{\rho}^d_{aq}(\mathbf{x}, t) + \dot{\rho}^r_{aq}(\mathbf{x}, t) \tag{13}$$

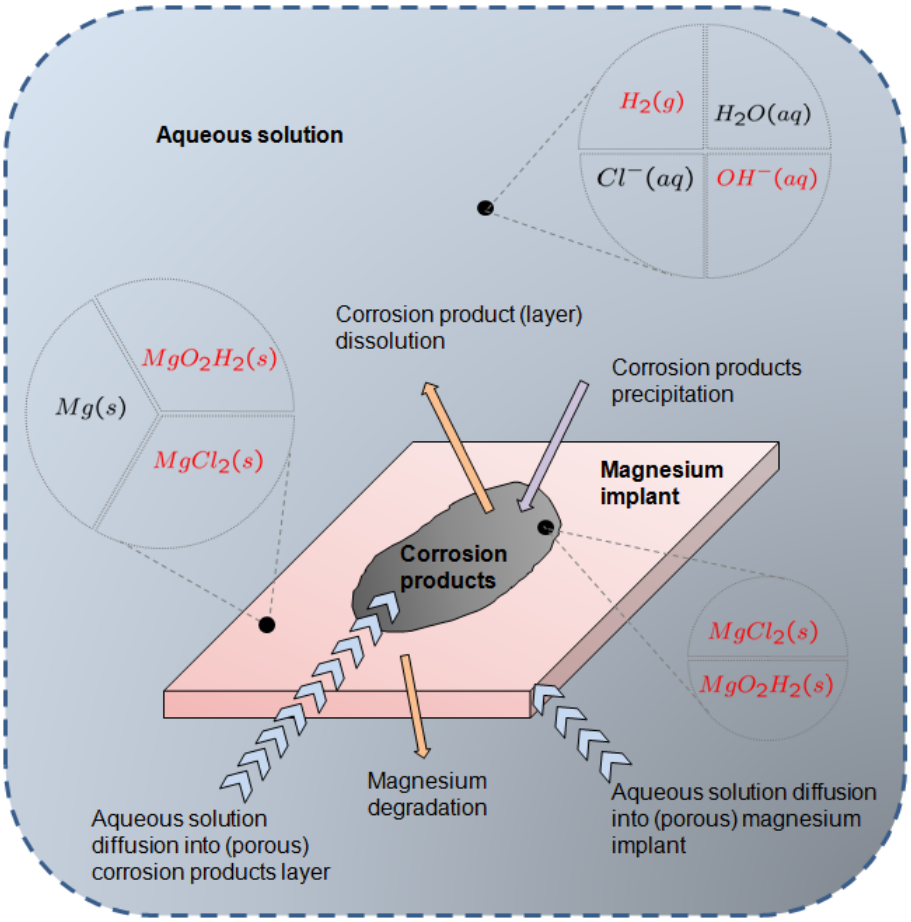

Figure 1. Sketch of the phenomenon of magnesium implants degradation. Species involved at different domains and description of physical processes. Species in red denote newly formed products during the process.

where $\dot{\rho}^d_{aq}$ and $\dot{\rho}^r_{aq}$ are the diffusive and reactive rates, respectively. On the one hand, $\dot{\rho}^d_{aq}$ is assumed as a fickean diffusion,

$$\dot{\rho}^d_{aq}(\mathbf{x}, t) = -\nabla \cdot (-D \nabla \rho_{aq}) \tag{14}$$

On the other hand,

$$\dot{\rho}_{aq}(\mathbf{x}, t) = \dot{\rho}_{H_2O} + \dot{\rho}_{H_2} + \dot{\rho}_{OH^-} + \dot{\rho}_{Cl^-} \tag{15}$$

and,

$$\dot{\rho}^r_{aq}(\mathbf{x},t) = \dot{\rho}^r_{H_2O} + \dot{\rho}^r_{H_2} + \dot{\rho}^r_{OH^-} + \dot{\rho}^r_{Cl^-} \tag{16}$$

ρ^r_{aq} is the reactive part of density ρ_{aq}. The relationship between density and concentration is $\dot{\rho}_{\square} = M_w(\square) \cdot [\dot{\square}]$, being $M_w(\square)$ the molecular weight of $\square$. Then, the terms involved in the right hand side of eq. (16) can be easily computed from eqs. (7),(9),(10) and (12). Finally, the complete model is written as:

$$\dot{\rho}_{aq} = -\nabla \cdot (-D\nabla\rho_{aq}) + \dot{\rho}^r_{H_2O} + \dot{\rho}^r_{H_2} + \dot{\rho}^r_{OH^-} + \dot{\rho}^r_{Cl^-} \quad \text{in} \quad \Omega(\mathbf{x},t)$$

$$\dot{\rho}_{H_2O} = -\nabla \cdot (-D\nabla\rho_{H_2O}) + \dot{\rho}^r_{H_2O} \quad \text{in} \quad \Omega(\mathbf{x},t)$$

$$\dot{\rho}_{H_2} = -\nabla \cdot (-D\nabla\rho_{H_2}) + \dot{\rho}^r_{H_2} \quad \text{in} \quad \Omega(\mathbf{x},t)$$

$$\dot{\rho}_{OH^-} = -\nabla \cdot (-D\nabla\rho_{OH^-}) + \dot{\rho}^r_{OH^-} \quad \text{in} \quad \Omega(\mathbf{x},t)$$

$$\dot{\rho}_{Cl^-} = -\nabla \cdot (-D\nabla\rho_{Cl^-}) + \dot{\rho}^r_{Cl^-} \quad \text{in} \quad \Omega(\mathbf{x},t)$$

$$\dot{\rho}^r_{H_2O} = 2 \cdot M_w(H_2O) \cdot \dot{\rho}_{Mg}/M_w(Mg) \quad \text{in} \quad \Omega(\mathbf{x},t)$$

$$\dot{\rho}^r_{H_2} = -M_w(H_2) \cdot \dot{\rho}_{Mg}/M_w(Mg) \quad \text{in} \quad \Omega(\mathbf{x},t)$$

$$\dot{\rho}_{Mg} = -k_d^{(1)} \cdot \rho_{Mg} \quad \text{in} \quad \Omega(\mathbf{x}, t) \tag{17}$$

$$\dot{\rho}^r_{OH^-} = M_w(OH) \cdot \dot{\rho}_{MgO_2H_2} / M_w(MgO_2H_2) \quad \text{in} \quad \Omega(\mathbf{x}, t)$$

$$\dot{\rho}^r_{Cl^-} = M_w(Cl) \cdot \dot{\rho}_{MgO_2H_2} / M_w(MgO_2H_2) \quad \text{in} \quad \Omega(\mathbf{x}, t)$$

$$\dot{\rho}^{diss}_{MgO_2H_2} = -k_d^{(2)} \cdot \rho_{MgO_2H_2} \quad \text{in} \quad \Omega(\mathbf{x}, t)$$

$$\dot{\rho}^{prec}_{MgO_2H_2} = -M_w(MgO_2H_2) \cdot \dot{\rho}_{Mg} / M_w(Mg) \quad \text{in} \quad \Omega(\mathbf{x}, t)$$

$$\dot{\rho}_{MgCl_2} = M_w(MgCl_2) \cdot \dot{\rho}_{MgO_2H_2} / M_w(MgO_2H_2) \quad \text{in} \quad \Omega(\mathbf{x}, t)$$

$$\dot{\rho}_{MgO_2H_2} = \dot{\rho}^{diss}_{MgO_2H_2} + \dot{\rho}^{prec}_{MgO_2H_2} \quad \text{in} \quad \Omega(\mathbf{x}, t)$$

The set of eqs. (18) is composed of 14 equations and 14 unknowns, namely, $\rho_{aq},\ \rho_{H_2O},\ \rho_{H_2},\ \rho_{OH^-},\ \rho_{Cl^-},\ \rho^r_{H_2O},\ \rho^r_{H_2},\ \rho^r_{OH^-},\ \rho^r_{Cl^-},\ \rho_{Mg},\ \rho_{MgO_2H_2},\ \rho^{diss}_{MgO_2H_2},\ \rho^{prec}_{MgO_2H_2},\ \rho_{MgCl_2}$. The problem is mathematically closed once prescribed boundary and initial conditions as follows:

- Boundary conditions:

$$\rho_{aq}(\mathbf{x} \in \Gamma, t) = \bar{\rho}_{H_2O} + \bar{\rho}_{H_2} + \bar{\rho}_{OH^-} + \bar{\rho}_{Cl^-} \tag{18}$$

- Initial conditions

$$\rho_{Mg}(\mathbf{x},0) = \bar{\rho}_{Mg} \quad \text{in} \quad \Omega(\mathbf{x},t)$$

$$\rho_{H_2O}(\mathbf{x},0) = 0$$

$$\rho_{H_2}(\mathbf{x},0) = 0$$

$$\rho_{OH^-}(\mathbf{x},0) = 0 \tag{19}$$

$$\rho_{Cl^-}(\mathbf{x},0) = 0$$

$$\rho_{MgCl_2}(\mathbf{x},0) = 0$$

$$\rho_{MgO_2H_2}(\mathbf{x},0) = 0$$

Eq. (18) is defined once the prescribed values of the aqueous solution (which depend on the aqueous medium), i.e. $\bar{\rho}_{H_2O}, \bar{\rho}_{H_2}, \bar{\rho}_{OH^-}, \bar{\rho}_{Cl^-}$, are known at the boundary of the biomaterial Γ. Moreover, initial conditions (19) are defined once the density of the biomaterial $\bar{\rho}_{Mg}$ is given. It is considered, without loss of generality, that neither aqueous solution nor corrosion products exist in the biomaterial at the beginning of the analysis. Other constants defined in the model are related to molecular weight of substances M_w which are easily known. Therefore only three model parameters are unknown *a priori*: diffusion coefficient of medium within magnesium D and kinetic constants k_d^1 and k_d^2. Even though we consider model parameters as fitting coefficients in this paper,

they are readily available by standard experimental measurement protocols. For the sake of simplicity, we considered $k_d = k_d^{(1)} = k_d^{(2)}$ along the results section.

The devoloped model is implemented in a finite element framework (3; 14; 26; 31). The numerical framework was previously described in a similar model in (27). Results are shown in the next section.

3 Results

3.1 Parametric analysis

In this section we implemented a magnesium square plate, $10 \times 10\ mm^2$ and $1\ mm$ thick, immersed in a salt solution. The details of the model are given in Fig. 2. A 2D finite element model was considered which neglects the thickness dimension. The corrosion and degradation of magnesium was simulated by means of the model presented in the previous section.

Results are presented in terms of magnesium mass loss (%), corrosion rate ($mm/year$), hydrogen release (mL/cm^2) and pH evolution. These quantities are defined as follows from model variables:

- Magnesium mass loss (%):

$$\frac{\bar{\rho}_{Mg} - m_{Mg}(t)/V_{Mg}}{\bar{\rho}_{Mg}} \cdot 100 \tag{20}$$

with $\bar{\rho}_{Mg} = 1.74\ g/cm^3$. V_{Mg} is the magnesium specimen volume, and

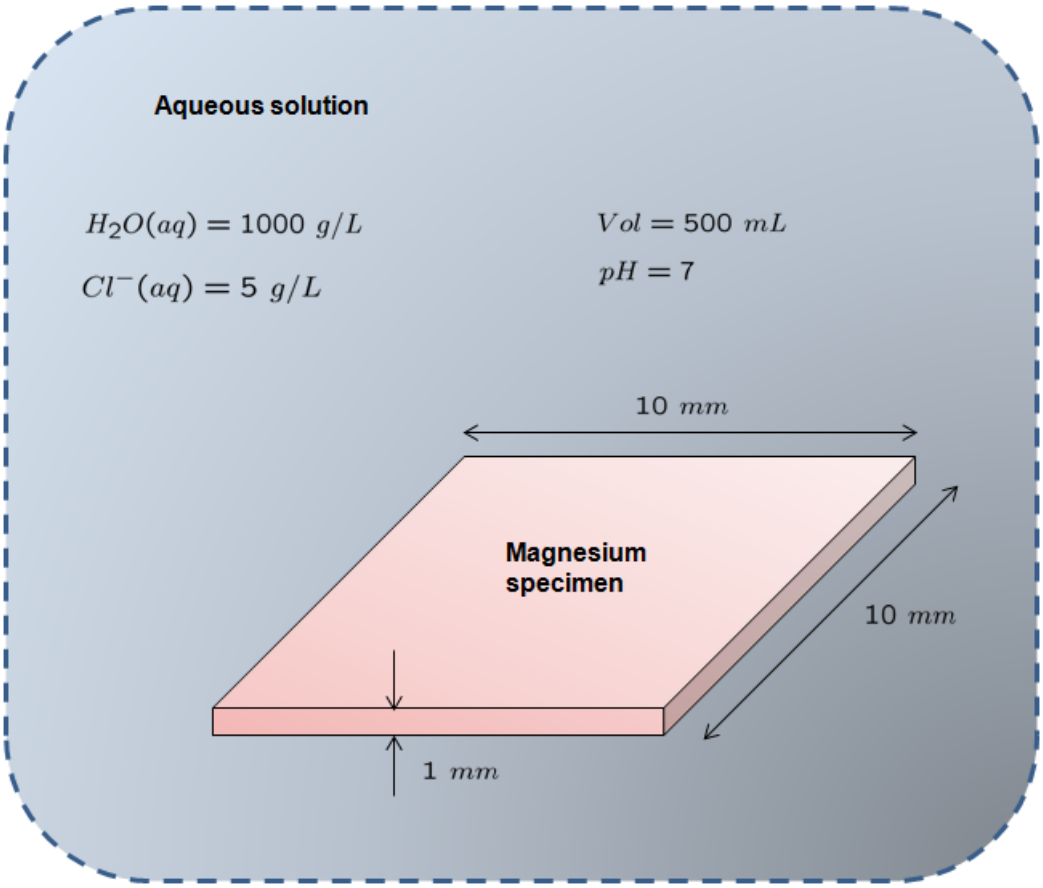

Figure 2. Problem statement of the example for parametric analysis.

$m_{Mg}(t)$ the overall magnesium mass of the specimen computed through the finite element model as:

$$m_{Mg}(t) = \sum_i^{NE} v_i \cdot \rho_{Mg}^i(t)$$

with NE and v_i being the number of elements and (tributary) volume of the finite element i of the element mesh, respectively. $\rho_{Mg}^i(t)$ is the magnesium density variable computed at those points.

- Corrosion rate ($mm/year$):

$$\frac{m_{Mg}(t) - m_{Mg}(t + \Delta t)}{\Delta t \cdot A \cdot \bar{\rho}_{Mg}} \tag{21}$$

Δt being the time step of the finite element simulation and A the surface area of the magnesium specimen.

- Hydrogen release (mL/cm^2)

$$\frac{m_{H_2}(t)}{\rho(H_2) \cdot A} \tag{22}$$

where $m_{H_2}(t)$ is the overall hydrogen release mass, computed in the finite element mesh analogously to magnesium mass above. $\rho(H_2)$ is the hydrogen density at room temperature and equal to 0.081 g/L.

- pH:

$$pH = 14 - pOH \tag{23}$$

where,

$pOH = -log([OH^-])$

with,

$[OH^-] = \frac{\rho_{OH-}}{M_w(OH^-)}$

A parametric analysis was conducted in order to explore the impact of model parameters D and k_d on model outcomes. D was considered to vary from $1-4{\cdot}10^{-4}$ (mm^2/day) which falls within the order of magnitude of the diffusion coefficient of compact (low porosity) materials (8). On the other hand, k_d was estimated in the range $2-8\cdot10^{-2}$ $(1/day)$ in order to obtain similar corrosion rates of experiments (19).

Results regarding to magnesium mass loss, corrosion rate, hydrogen release and pH evolution quantities are plotted in Fig. 3 for different values of D and k_d. Furthermore, mass loss and corrosion product variables are plotted in Figs. 4 and 5, respectively. Since the evolution of variables is uniform along the specimen, only a small region around the edge of the specimen is plotted.

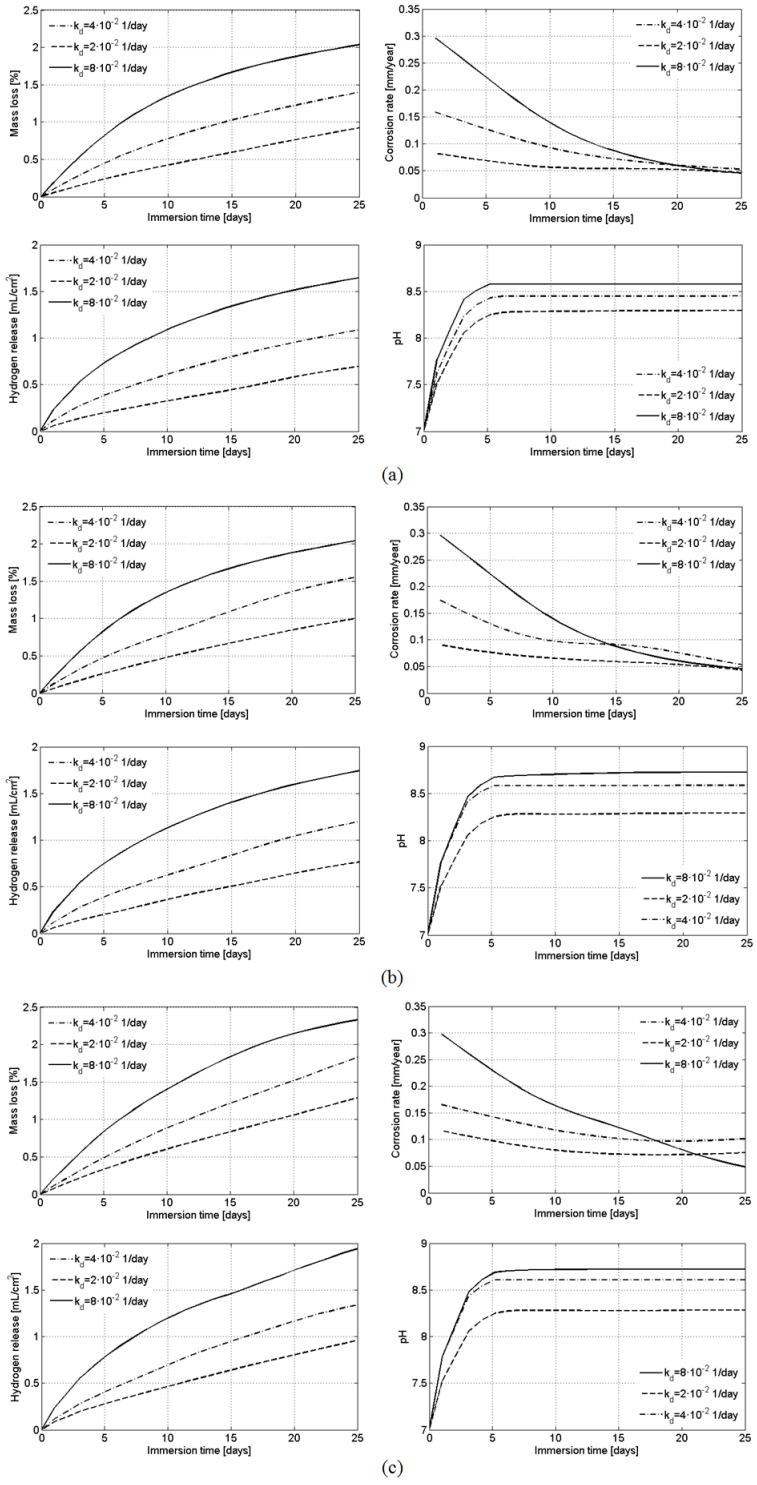

Figure 3. Magnesium mass loss, corrosion rate, hydrogen release and pH evolution quantities: Parametric analysis. (a) $D = 1 \cdot 10^{-4}$ (mm^2/day), (b) $D = 2 \cdot 10^{-4}$ (mm^2/day) and (c) $D = 4 \cdot 10^{-4}$ (mm^2/day).

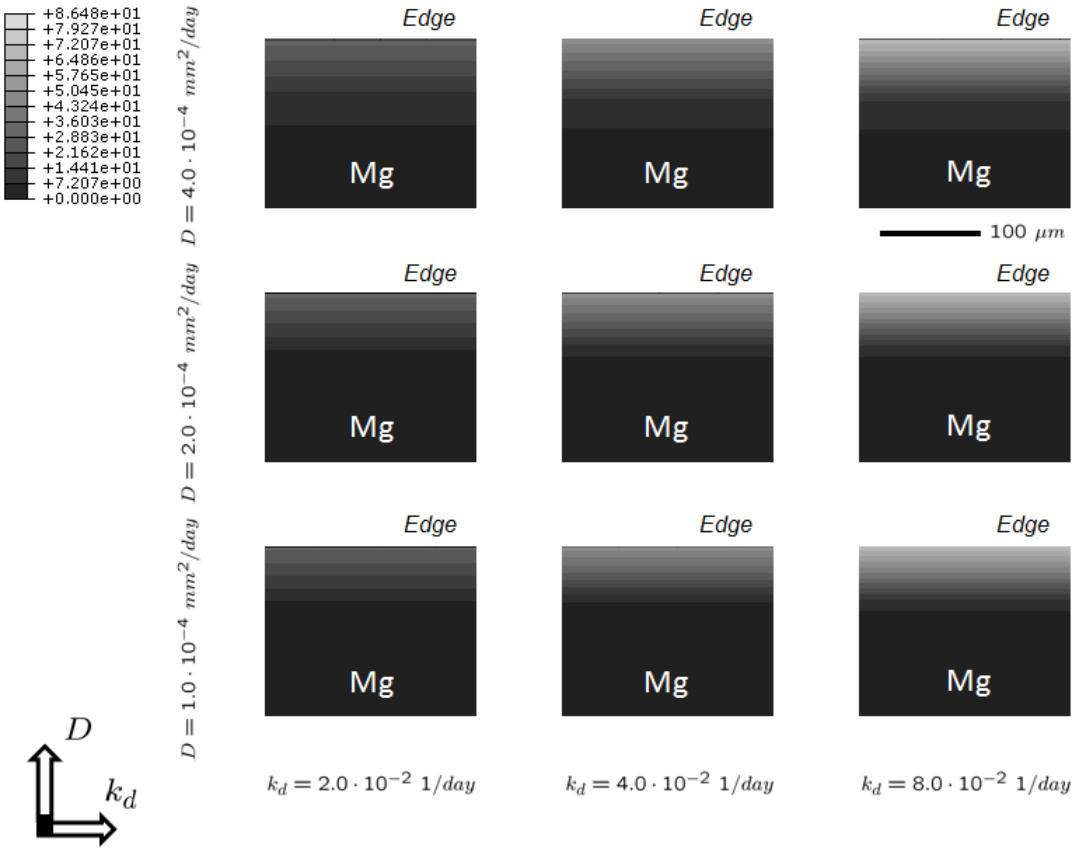

Figure 4. Mass loss chart (data in %) at the edge region of the magnesium specimen (see Fig. 2) at the end of the analysis (25 days). Parametric matrix of analyzed values for D and k_d.

3.2 Example of application 1

In this example of application, the *in vitro* corrosion test presented in Seitz et al. (28) is reproduced and simulated. Then, neodymium-containing magnesium alloy MgNd2 specimens having a length of 25 mm and diameter of 2.5 mm were immersed in 700 mL of SBF solution (see details of the composition of the solution in (28)). A 2D axisymmetric model was used. Mass loss and corrosion rate were recorded along 25 days of immersion (28).

The results of the simulation of this experimental test is compared in Fig.

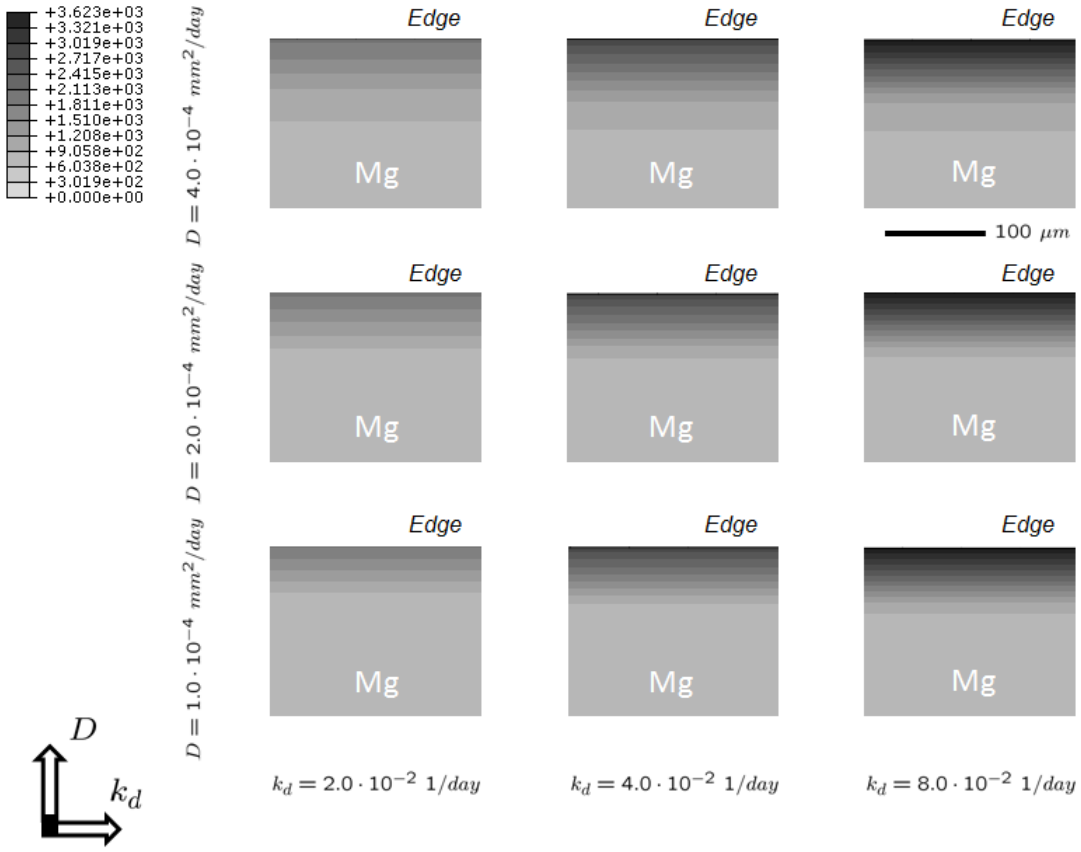

Figure 5. Corrosion products ($\rho_{MgO_2H_2} + \rho_{MgCl_2}$) chart (data in g/L) at the edge region of the magnesium specimen (see Fig. 2) at the end of the analysis (25 days). Parametric matrix of analyzed values for D and k_d.

6 in terms of mass loss and corrosion rate. These quantities were computed from the definition in eqs. (20) and (21). The model parameters were fitted to $D = 1.6 \cdot 10^{-4}\ (mm^2/day)$ and $k_d = 8.4 \cdot 10^{-2}\ (1/day)$.

3.3 Example of application 2

In order to explore the availability of the presented model for *in vivo* applications, where higher corrosion rates are found, the animal test presented in Li et al. (20) is reproduced and simulated. In this test, magnesium screw alloys (Mg-Zn-Zr) were implanted in adult Japanese white rabbits (see Fig. 7). The

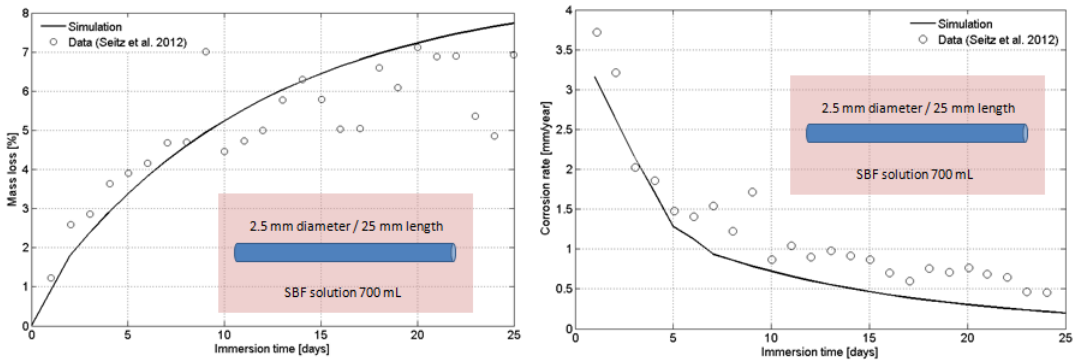

Figure 6. Mass loss (left) and corrosion rate (right) simulation of the experimental test presented in (28).

evolution and degradation of the geometry of the screws was recorded along the implantation time (6 months) by means of micro-computed tomography (20).

On the other hand, the geometry of the screw was approximated and modeled by using a 2D axisymmetric model as a first approach. Due to the lack of data and complexity to get information about the *in vivo* fluid environment, a chloride concentration of 5 g/L was considered in the model, as in the previous example. This parameter has no influence on the specific analyzed variables in this case, as discussed in the next section. The model parameters were fitted for this example to $D = 1.6 \cdot 10^{-4}$ (mm^2/day) and $k_d = 3.4 \cdot 10^{-1}$ $(1/day)$.

Results regarding mass loss and corrosion rate are presented in Fig. 7. As in the previous examples, these quantities were computed from their definition in eqs. (20) and (21). Finally, the evolution of the degradation of the screw magnesium geometry is presented in Fig. 8 both for simulation results and experimental comparison.

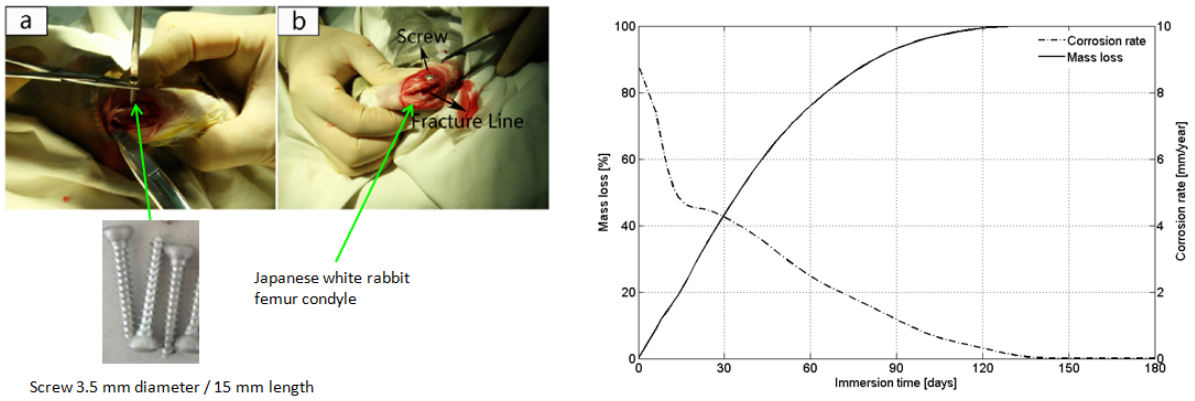

(a) (b)

Figure 7. Left: *In vivo* magnesium screw implantation for degradation experiment (20). Right: Mass loss and corrosion rate simulation of the experimental test presented in (20).

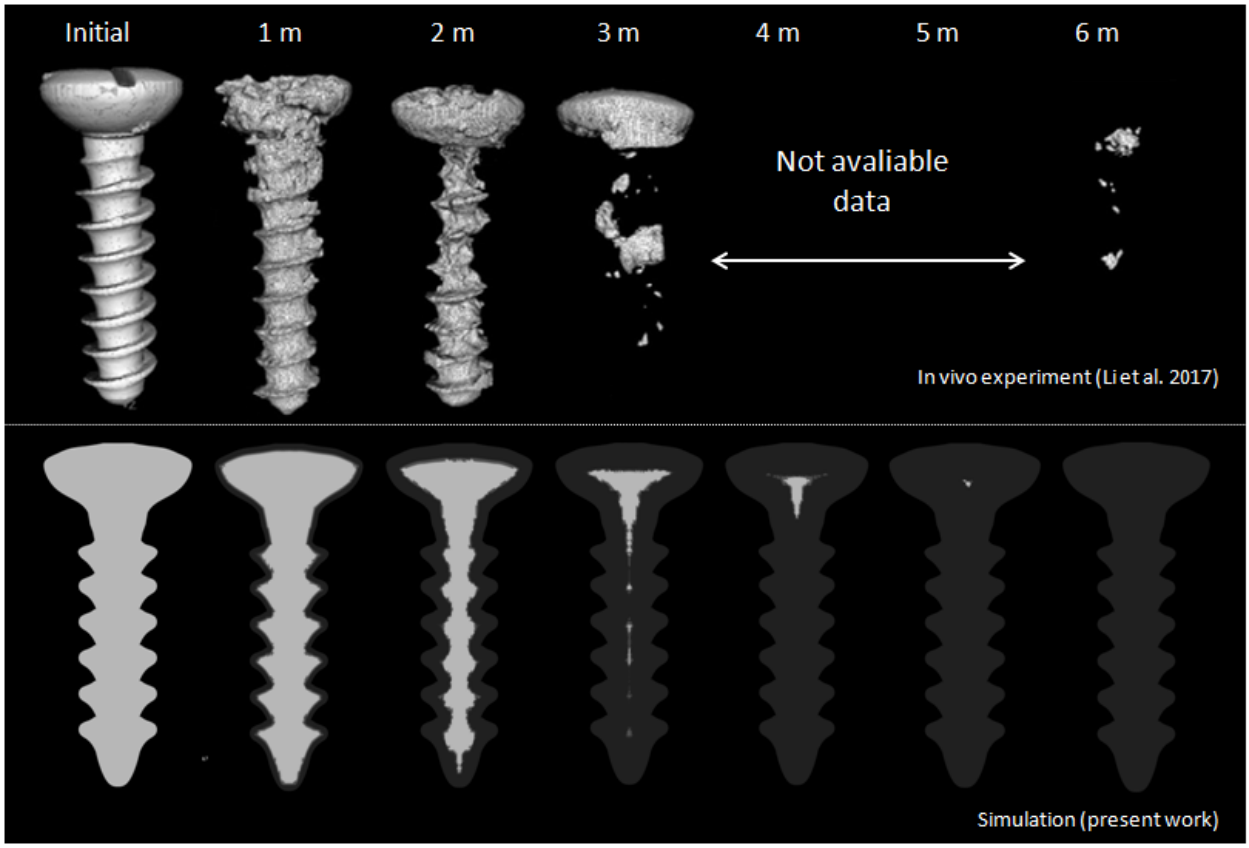

Figure 8. *In vivo* magnesium screw degradation map along time (6 months) (20) and comparison with computer simulation.

4 Discussion

The analysis of the results presented in the previous section allows to discuss several interesting points.

Firstly, the parametric analysis in Fig. 3 was established in the range of compact (low porosity) metals and slow corrosion rate. At this range, evolution of analyzed variables i.e. magnesium mass loss, corrosion rate, hydrogen release and pH fall within the order of magnitude and trend of experimental measurements for these quantities (1; 17; 20; 22) to cite a few. Although the model was validated with two specific applications, a proper fitting of model parameters may reproduce any of the reported experimental observations.

In the range of analyzed values for the diffusion coefficient and kinetic constant, it is seen in Fig. 3 that a higher kinetic rate yields to a higher consumption of magnesium (and hence faster corrosion rate) as well as an increase in the release of ionic substances. However, in the range of analyzed values, diffusion coefficient has a minor effect on model outcomes. This conclusion is achieved just analyzing the impact of parameter D on curves shown in Fig. 3. Moreover, Figs. 4 and 5 show that the corrosion activity is produced in a close layer region near to the surface of the implant. The order of magnitude of this layer is 100 μm (see Figs. 4 and 5). Consequently, aqueous solution diffusion within the implant may be neglected for compact (low porosity) magnesium as a first approach. However, the presented model in this paper is general and allows to simulate porous metals (scaffolds) in different applications such as tissue engineering problems.

On the other hand, the established model allows the analysis of pH evolution

as a model variable. For the analyzed cases, pH is dependent on hydroxide release (as a consequence of reaction equations) and aqueous solution composition (chloride and initial pH). Secondary reactions which involve the hydroxide ions were not considered in the model. Moreover, some magnesium coatings biomaterials include oxide release (11) which should be considered in the formulation in order to properly reproduce the pH evolution. The effect of the aqueous solution in the model is only related to pH evolution according to the main considered reaction equations in (1), (2) and (3).

The analysis of the results in the different examples of application allows to conclude that the model captures well the observed experimental trends of magnesium degradation, both *in vitro* (section 3.2) and *in vivo* (section 3.3). The effect of *in vitro* versus *in vivo* is considered phenomenologically in the model through the kinetic constant k_d. Therefore, different effects such as fluid circulation or fluid environment composition are considered in this parameter under the meaning of a catalytic effect in the chemical reactions. Consequently, the effect of different solutions on magnesium corrosion may be indirectly incorporated in the model through k_d. The fitted values and results of *in vitro* and *in vivo* scenarios give a ratio of 4 times faster for degradation *in vivo*. This value is within the order of magnitude of reported works (19; 20). It allows to conclude that the model is valid both for slow and fast degradation rate regimes.

Future work of the preliminary development and analysis presented in this paper includes, firstly, a thorough experimental validation of the proposed model. Secondly, the model allow to couple the corrosion modeling to the mechanical behavior of magnesium-based implants. In this sense, the model would turn into a multiphysics approach available to simulate the evolution of

the degradation of mechanical behavior of implants as the phenomenological consequence of corrosion in a coupled way.

5 Aknowledgements

The authors gratefully acknowledge the Ministerio de Economía y Competitividad del Gobierno España (DPI2014-58233-P) for research funding.

References

[1] Abidin N.I.Z., B. Rolfe, H. Owen, J. Malisano, D. Martin, J. Hofstetter, P.J. Uggowitzer, and A. Atrens. The in vivo and in vitro corrosion of high-purity magnesium and magnesium alloys WZ21 and A91. Corros Sci. 75:354-366, 2013.

[2] Bajger P., J.M.A. Ashbourn, V. Manhas, Y. Guyot, K. Lietaert, and L. Geris. Mathematical modelling of the degradation behaviour of biodegradable metals. Biomech Model Mechanobiol. 16:227-238, 2017.

[3] Bathe, K.J. Finite Element Procedures, Prentice-Hall, New Jersey, 1996.

[4] Brar H.S., M.O. Platt, M. Sarntinoranont, P.I. Martin, and M.V. Manuel. Magnesium as a biodegradable and bioabsorbable material for medical implants, JOM. 61:31-34, 2009.

[5] Castellani C., R.A. Lindtner, P. Hausbrandt, E. Tschegg, S.E. Stanzl-Tschegg, G. Zanoni, S. Beck, and A.M. Weinberg. Bone-implant interface strength and osseointegration: biodegradable magnesium alloy versus standard titanium control. Acta Biomater. 7:432-440, 2011.

[6] Choudhary L., and R.K. Singh Raman. Magnesium alloys as body im-

plants: fracture mechanism under dynamic and static loadings in a physiological environment. Acta Biomater. 8:916-923, 2012.

[7] Cooper L.F., Y. Zhou, J. Takebe, J. Guo, A. Abron, A. Holmen, and J.E. Ellingsen. Fluoride modification effects on osteoblast behavior and bone formation at TiO2, grit-blasted c.p. titanium endosseous implants, Biomaterials. 27:926-936, 2006.

[8] Grassman P. Physical Principles of Chemical Engineering (International series of monographs in chemical engineering, v. 12) [1st English ed.] Edition.

[9] Grogan J.A., B.J. O Brien, S.B. Leen, and P.E. McHugh. A corrosion model for bioabsorbable metallic stents. Acta Biomater. 7:3523-3533, 2011.

[10] Grogan J.A., S.B. Leen, and P.E. McHugh. A physical corrosion model for bioabsorbable metal stents. Acta Biomater. 10:2313-2322, 2014.

[11] Gu X.N., N. Li, W.R. Zhou, Y.F. Zheng, X. Zhao, Q.Z. Cai, and L.Q. Ruan. Corrosion resistance and surface biocompatibility of a microarc oxidation coating on a Mg-Ca alloy, Acta Biomater. 7:1880-1889, 2011.

[12] Haude M., R. Erbel, P. Erne, S. Verheye, H. Degen, D. Bose, P. Vermeersch, I. Wijnbergen, N. Weissman, F. Prati, R. Waksman, and J. Koolen. Safety and performance of the drug-eluting absorbable metal scaffold (dreams) in patients with de-novo coronary lesions: 12 month results of the prospective, multicentre, first-in-man BIOSOLVE-I trial. Lancet. 381:836-844, 2013.

[13] Hollister S.J. Porous scaffold design for tissue engineering. Nat. Mater. 4:518-524, 2005.

[14] Hughes T.J.R. The Finite Element Method: Linear Static and Dynamic Finite Element Analysis, McGraw-Hill (second edition), Dover, New York, 2000.

[15] Jafari S., R.K. Singh Raman, and C.H.J. Davies. Corrosion fatigue of a magnesium alloy in modified simulated body fluid, Eng. Fract. Mech. 137:2-11, 2015.

[16] Kannan M.B., and R.K. Singh Rama. In vitro degradation and mechanical integrity of calcium-containing magnesium alloys in modified-simulated body fluid, Biomaterials. 29:2306-2314, 2008.

[17] Krämer M., M. Schilling, R. Eifler, B. Hering, J. Reifenrath, S. Besdo, H. Windhagen, E. Willbold, and A. Weizbauer. Corrosion behavior, biocompatibility and biomechanical stability of a prototype magnesium-based biodegradable intramedullary nailing system. Materials Science and Engineering. C. 59:129-135, 2016.

[18] Kraus T., S.F. Fischerauer, A.C. Hänzi, P.J. Uggowitzer, J.F. Löffler, and A.M. Weinberg. Magnesium alloys for temporary implants in osteosynthesis: in vivo studies of their degradation and interaction with bone. Acta Biomater. 8:1230-1238, 2012.

[19] Li X., X. Liu, S. Wu, K.W.K. Yeung, Y. Zheng, and P.K. Chu. Design of magnesium alloys with controllable degradation for biomedical implants: From bulk to surface. Acta Biomater. 45:2-30, 2016.

[20] Li Z., S. Sun, M. Chen, B.D. Fahlman, D. Liu, and H. Bi. In vitro and in vivo corrosion, mechanical properties and biocompatibility evaluation of MgF2-coated Mg-Zn-Zr alloy as cancellous screws. Materials Science and Engineering C. 75:1268-1280, 2017.

[21] Liu Y.J., Z.Y. Yang, L.L. Tan, H. Li, and Y.Z. Zhang. An animal experimental study of porous magnesium scaffold degradation and osteogenesis. J. Med. Biol. Res. 47:715-720, 2014.

[22] Myrissa A., N.A. Agha, Y. Lu, E. Martinelli, J. Eichler, G. Szakacs, C. Kleinhans, R. Willumeit-Römer, U. Schäfer, and A. Weinberg. In vitro and

in vivo comparison of binary Mg alloys and pure Mg. Materials Science and Engineering C. 61:865-874, 2016.

[23] Pichler K., S. Fischerauer, P. Ferlic, E. Martinelli, H.P. Brezinsek, P.J. Uggowitzer, J.F. Loffler, and A.M. Weinberg. Immunological response to biodegradable magnesium implants. JOM. 66:573-579, 2014.

[24] Poinern G.E.J., S. Brundavanam, and D. Fawcett. Biomedical Magnesium Alloys: A Review of Material Properties, Surface Modifications and Potential as a Biodegradable Orthopaedic Implant. American Journal of Biomedical Engineering. 2:218-240, 2012.

[25] Raimund E., D.M. Carlo, B. Jozef, J. Bonnier, B. de Bruyne, F.R. Eberli, P. Erne, M. Haude, B. Heublein, M. Horrigan, C. Ilsley, D. Bose, J. Koolen, T.F. Luscher, N. Weissman, and R. Waksman. Temporary scaffolding of coronary arteries with bioabsorbable magnesium stents: a prospective, non-randomised multicentre trial. Lancet. 369:1869-1875, 2007.

[26] Reddy J.N. An Introductory Course to the Finite Element Method, McGraw-Hill (second edition), Boston, 1993.

[27] Sanz-Herrera J.A., and A.R. Boccaccini. Modelling bioactivity and degradation of bioactive glass based tissue engineering scaffolds. Int J Solids Struc. 48:257-268, 2011.

[28] Seitz J.M., R. Eifler, J. Stahl, M. Kietzmann, and Fr.W. Bach. Characterization of MgNd2 alloy for potential applications in bioresorbable implantable devices. Acta Biomaterialia. 8:3852-3864, 2012.

[29] Song G. Control of biodegradation of biocompatible magnesium alloys, Corros. Sci. 49:1696-1701, 2007.

[30] Staiger M.P., A.M. Pietak, J. Huadmai, and G. Dias. Magnesium and its alloys as orthopedic biomaterials: a review. Biomaterials. 27:1728-1734, 2006.

[31] Zienkiewicz O.C., and R.L. Taylor. The Finite Element Method, Butterworth-Heinemann (fifth edition), Oxford, 2000.

[32] Windhagen H., K. Radtke, A. Weizbauer, J. Diekmann, Y. Noll, U. Kreimeyer, R. Schavan, C. Stukenborg-Colsman, and H. Waizy. Biodegradable magnesium-based screw clinically equivalent to titanium screw in hallux valgus surgery: short term results of the first prospective, randomized, controlled clinical pilot study. BioMed. Eng. OnLine. 12:62, 2013.

[33] Witte F., N. Hort, C. Vogt, S. Cohen, K.U. Kainer, R. Willumeit, and F. Feyerabend. Degradable biomaterials based on magnesium corrosion. Curr Opin Solid State Mater Sci. 12:63-72, 2008.

[34] Witte F. The history of biodegradable magnesium implants: a review, Acta Biomater. 6:1680-1692, 2010.

[35] Wu S.L., X.M. Liu, K.W.K. Yeung, C.S. Liu, and X.J. Yang. Biomimetic porous scaffolds for bone tissue engineering. Mat. Sci. Eng. R 80:1-36, 2014.

[36] Ye X.Y., M.F. Chen, C. You, and D.B. Liu. The influence of hf treatment on corrosion resistance and in vitro biocompatibility of Mg-Zn-Zr alloy. Front. Mater. Sci. Chin. 4:132-138, 2010.

[37] Zeng R.C., W.C. Qi, H.Z. Cui, F. Zhang, S.Q. Li, and E.H. Han. In vitro corrosion of asextruded Mg-Ca alloys-the influence of Ca concentration, Corros. Sci. 96:23-31, 2015.